

“Quantum-optical coherence tomography” with classical light

J. Lavoie, R. Kaltenbaek, and K. J. Resch*

*Institute for Quantum Computing and Department of Physics & Astronomy,
University of Waterloo, Waterloo, Canada, N2L 3G1*

Quantum-optical coherence tomography (Q-OCT) is an interferometric technique for axial imaging offering several advantages over conventional methods. Chirped-pulse interferometry (CPI) was recently demonstrated to exhibit all of the benefits of the quantum interferometer upon which Q-OCT is based. Here we use CPI to measure axial interferograms to profile a sample accruing the important benefits of Q-OCT, including automatic dispersion cancellation, but with 10 million times higher signal. Our technique solves the artifact problem in Q-OCT and highlights the power of classical correlation in optical imaging.

INTRODUCTION

Optical coherence tomography (OCT) [1] is a non-invasive imaging technique using low-coherence interferometry to produce depth profiles of a sample. OCT has found many biomedical applications; prominent examples include the diagnosis of ocular diseases or detection of early-stage cancer [2]. Axial resolution in OCT is ultimately limited by the coherence length of the light source and can be less than $1\text{ }\mu\text{m}$ for very broadband sources [3]. This resolution is hindered by material dispersion which both broadens the features in the interferograms and reduces the contrast.

Exciting developments in quantum interferometry led to the proposal and demonstration of quantum-optical coherence tomography (Q-OCT) [4, 5]. This technique replaces white-light interferometry (WLI) with Hong-Ou-Mandel (HOM) interferometry [6] utilizing frequency-entangled photon pairs. This device automatically cancels all even orders of dispersion in the resulting interferogram, including group-velocity dispersion, the most significant contribution [7]. Dispersion cancellation in HOM interference is “blind”, requiring no *a priori* knowledge of the material properties, in contrast with dispersion compensation methods (see [2] and references therein). In addition to dispersion cancellation, the HOM interferometer is phase insensitive, has better resolution than WLI with the same bandwidth, and the interference visibility is insensitive to unbalanced loss. Unfortunately, this technique is based on entangled photon pairs and the costs, in terms of speed and expense, have limited its widespread adoption. Other techniques for blind dispersion compensation without entanglement have been proposed [8, 9] or demonstrated [10], but they require unavailable technology [8] or significant numerical post-processing [9, 10] and do not have the other advantageous properties of Q-OCT. We have recently demonstrated a completely classical technique, based on oppositely-chirped laser pulses, for producing an interferogram with *all* the advantages of HOM interference with vastly higher signal [11].

In the present work, we use chirped-pulse interferometry (CPI) for axial profiling a sample with two optical interfaces. Q-OCT interferograms have been shown to contain artifacts [4], signals that do not correspond to real features of the sample. Due to the strong analogy, these artifacts also appear in CPI-based axial imaging. We experimentally demonstrate a straightforward method for controlling these artifacts. Although it is possible to control these

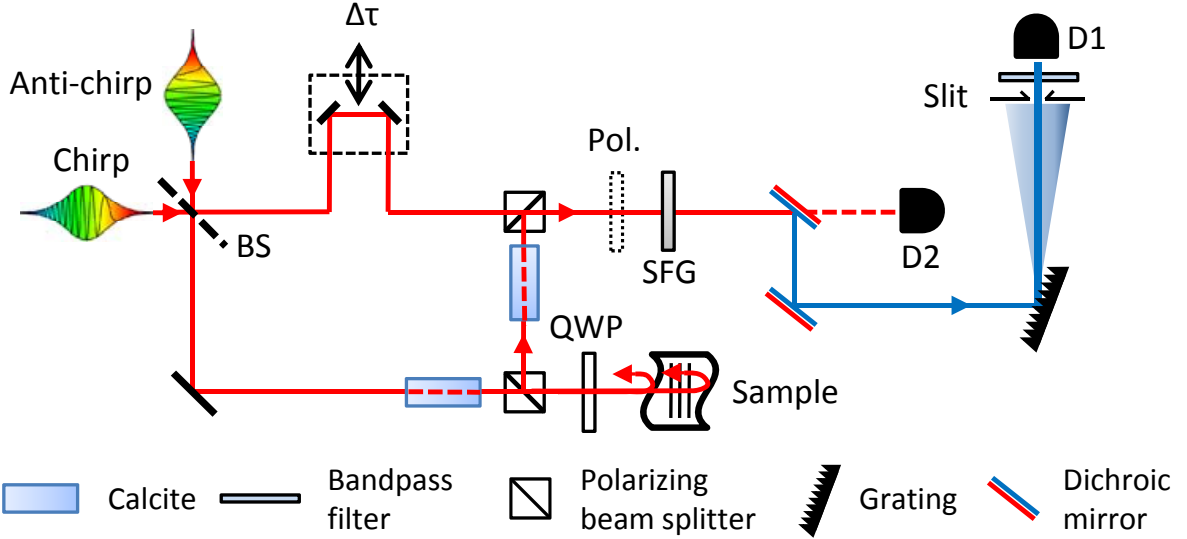


FIG. 1: Experimental setup for axial profiling with chirped-pulse interferometry. Pairs of oppositely-chirped laser pulses with horizontal polarization are combined at a 50/50 beam splitter (BS). The light from one BS output reflects from a sample; the light from the other undergoes a spatial delay. In the sample arm, two passes through the quarter-wave plate (QWP) rotate the polarization to vertical. This allows spatial recombination of the two beams at a polarizing beam splitter. Both beams are focussed onto a 0.5 mm thick BBO crystal phase-matched for type-II sum-frequency generation (SFG). Dichroic mirrors separate the fundamental from the SFG light. A grating and slit are used to filter a narrow band (0.46 nm FWHM) of SFG light before the light is detected by an amplified Si photodetector (D1). An alternate configuration, where a 45° polarizer is inserted before the nonlinear crystal and the fundamental light is directly detected with a photodiode (D2), allows the observation of white-light fringes and a direct comparison with CPI. A pair of calcite blocks can be inserted to compare the effects of material dispersion on the interferograms.

artifacts in Q-OCT as well [4], it is technically challenging and has not been demonstrated.

EXPERIMENTAL SETUP AND METHODS

Our interferometer is shown in Fig. 1 and described in the caption. It relies on pairs of oppositely-chirped laser pulses that have been stretched to several hundred times their initial, transform-limited, pulse duration. In this large-chirp limit, at any given time the two frequency-anticorrelated pulses have frequencies $\omega_0 + \Omega$ and $\omega_0 - \Omega$, respectively. Here, ω_0 is the average of the instantaneous frequencies of these pulses. If the chirped pulses are coincident at the input beam splitter, ω_0 is equal to the centre frequency of the laser, but it can be tuned by changing the relative delay between the pulses. We refer to ω_0 as the *operating frequency* to distinguish it from the centre frequency of the laser. Following the theoretical framework from [4], we assume that the effect of the sample is modelled by a linear transfer function, $H(\Omega)$. The reference arm contains an adjustable path delay, $\Delta\tau$.

After propagation in each arm, the beams undergo sum-frequency generation (SFG) in a nonlinear medium. We detect SFG light in a very narrow frequency band near $2\omega_0$ ensuring that the output signal is almost exclusively due to cross-correlations between the chirped and anti-chirped pulses. Under these conditions, the signal integrated over all frequencies in the chirped pulses and measured by a square-law detector, $S(\Delta\tau)$, is

$$S(\Delta\tau) \propto \int d\Omega I(\Omega)I(-\Omega)|H(\Omega)|^2 - \text{Re} \left[\int d\Omega I(\Omega)I(-\Omega)H(\Omega)H^*(-\Omega)e^{-2i\Omega\Delta\tau} \right], \quad (1)$$

where $I(\Omega)$ is the intensity spectrum of both laser pulses. The CPI signal is identical to that in Q-OCT when $I(\Omega)I(-\Omega)$ is equal to the spectrum of the entangled photons (see [4], Eqns. (6)-(8)).

A mode-locked Ti:Sapphire laser (center wavelength 790 nm, average power 2.7 W, repetition rate 80 MHz) was used to create a pair of horizontally-polarized beams of oppositely-chirped pulses using a grating-based stretcher and compressor [12]. These stretched the initial pulses from 100 fs to 54 ps (48 ps) with 11 nm (10 nm) bandwidth for the chirped (anti-chirped) pulses. Note that the difference in the pulse duration is due to slightly different bandwidths, not different chirp rates. Details on the stretcher and compressor can be found in [11].

RESULTS AND DISCUSSIONS

We used a borosilicate microscope coverglass as the sample. The CPI (WLI) data was taken by recording the signal of detector D1 (D2) over the delay $\Delta\tau$. In each scan data was accumulated for 0.5 s over a range of 0.5 mm. The data without and with the calcite blocks are shown in Fig. 2(a) and Fig. 2(b), respectively, where the upper (lower) plots are CPI (WLI) scans. Without additional dispersion (Fig. 2(a)), the CPI interference dips have widths of $20.1 \pm 0.3 \mu\text{m}$ and $20.6 \pm 0.4 \mu\text{m}$ FWHM and corresponding visibilities of 39.0% and 40.9% for the front and the back surface of the coverglass, respectively. The WLI patterns have widths $30.4 \pm 0.3 \mu\text{m}$ and $29.9 \pm 0.3 \mu\text{m}$ FWHM and corresponding visibilities of 12.9% and 14.0%. The errors in these measurements are mainly due to positioning uncertainty of the motor. Even without the addition of calcite blocks, we see that the CPI signal has enhanced resolution by a factor of 1.5 compared to WLI. This enhancement factor is slightly larger than the theoretically expected value of $\sqrt{2}$ (assuming Gaussian spectra), due to uncompensated dispersion caused by the additional PBS in the sample arm.

The average optical power in the WLI scans in Figs. 2(a) & 2(b) was ~ 10 mW. In the CPI scans, the normalized intensity of 1.0 corresponds to $0.3 \mu\text{W}$ of measured optical power. This corresponds to approximately 10^{12} photons/s. It is difficult to directly compare this rate with the performance of Q-OCT demonstrated in [5] since only normalized rates are presented; however, the highest measured coincidence-counting rate from an entangled photon source to date is $\sim 10^6$ photons/s [13]. Given a total sample reflectivity of $\sim 10\%$ our measured power is 7 orders of magnitude larger than what could be achieved in Q-OCT with the best available technology.

The path delay between the two CPI interference dips is $286.1 \pm 0.4 \mu\text{m}$. The operating frequency was measured by taking the spectrum of the light after the first beam splitter; it is the frequency at which the chirped and antichirped pulses interfere. The observed delay can be converted to the thickness of the coverslip by dividing by the group index, $n_g(\lambda) =$

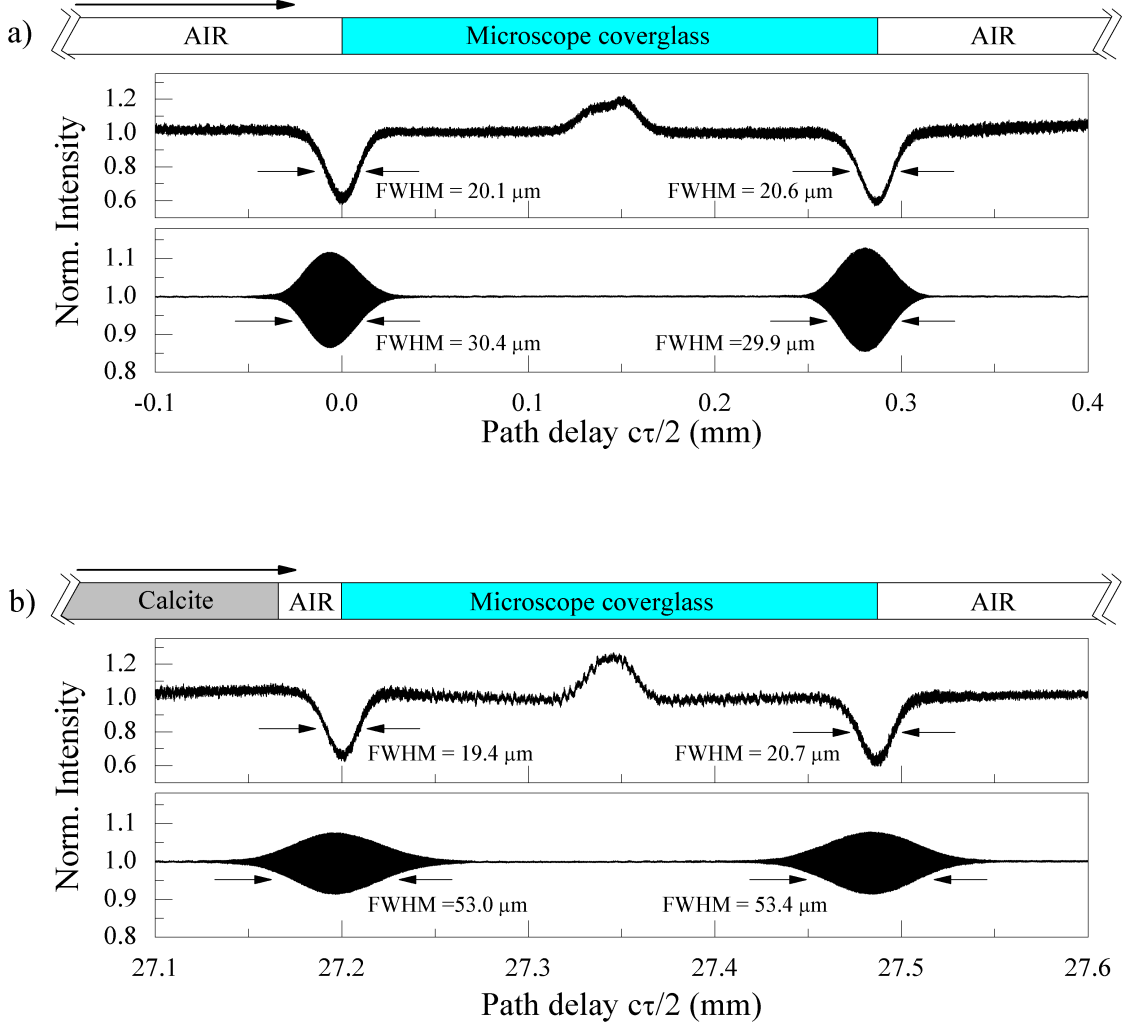


FIG. 2: Axial scans of a microscope coverglass using chirped-pulse and white-light interference. Light enters from the left and is reflected from either the front or the back surface of the sample, as indicated at the top of the figure. The normalized detector signal is plotted as a function of path delay. Each data set shows interference features corresponding to the front and back surface reflections of the sample. The CPI (top) and the WLI (bottom) were taken a) without and b) with calcite blocks. The CPI signal resolution, as measured by the width of the interference feature, is unaffected by the dispersion whereas the WLI is broadened by 74%. As in Q-OCT, CPI shows an artifact between the two real signals.

$n(\lambda) - \lambda \frac{dn}{d\lambda}\bigg|_{\lambda}$, of borosilicate glass at the operating wavelength 790.8 ± 0.3 nm, $n_g = 1.53482$ [14]. The optical measurement of the coverglass thickness is 186.4 ± 0.3 μm which is in good agreement with a direct measurement, using a micrometer, yielding 186.4 ± 0.8 μm .

To investigate the effects of material dispersion on the interference, we added a pair of calcite beam displacers into the setup. The sum of their lengths is 80.58 ± 0.01 mm and the

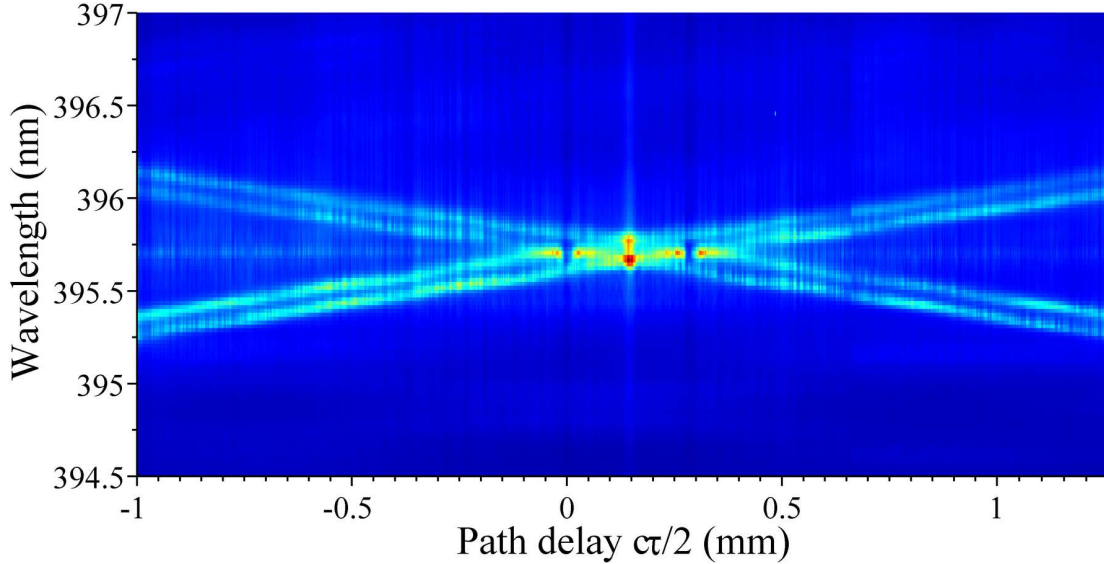


FIG. 3: False-color representation of the SFG spectrum vs path delay. Two pairs of narrow lines originate from SFG of the oppositely-chirped laser pulses with different time delays. When the time delay through the reference arm coincides with the delay through the sample arm from one of the two interfaces, an interference dip occurs. The other pair of crossings between the real interference dips gives rise to the artifact.

light propagates through them with ordinary polarization. The widths of the CPI dips are unchanged at $19.4 \pm 0.6 \mu\text{m}$ and $20.7 \pm 0.4 \mu\text{m}$ FWHM; the WLI envelopes are significantly broadened by 74% to $53.0 \pm 0.3 \mu\text{m}$ and $53.4 \pm 0.3 \mu\text{m}$. Under these conditions, CPI has a factor of 2.65 better resolution than WLI.

Both CPI and Q-OCT signals contain artifacts, additional features in the interferograms that do not correspond to real interfaces. These can be seen in the data in Fig. 2 in between the interference dips. To illuminate the origin of these features in CPI we measured the full SFG spectrum as a function of delay using a high-resolution spectrometer (ACTON SP-2758). The results are shown in Fig. 3. On this scale, the only features visible are due to cross-correlations; the autocorrelations form a weak, broadband background. When the paths are unbalanced, the signal contains two doublets of narrow spectral lines. One of these doublets is due to the chirped pulse traversing the sample arm and the anti-chirped pulse traversing the reference. The two peaks of the doublet are separated in frequency due to the difference in optical delay reflecting from the front and back surface of the sample. When the chirped pulse is reflected from the front surface the frequency of the cross-correlation will be slightly higher than upon reflection from the back surface. The other doublet can be understood by swapping the roles of the chirped and anti-chirped pulses.

Changing the path delay changes the spacing between the two doublets. An interference dip occurs when the delay in the reference path is equal to a delay in the sample path. The interference results from two different processes (chirp in one of the two arms and anti-chirp in the other) each producing light at the same frequency, but out of phase. In Fig. 3 the four

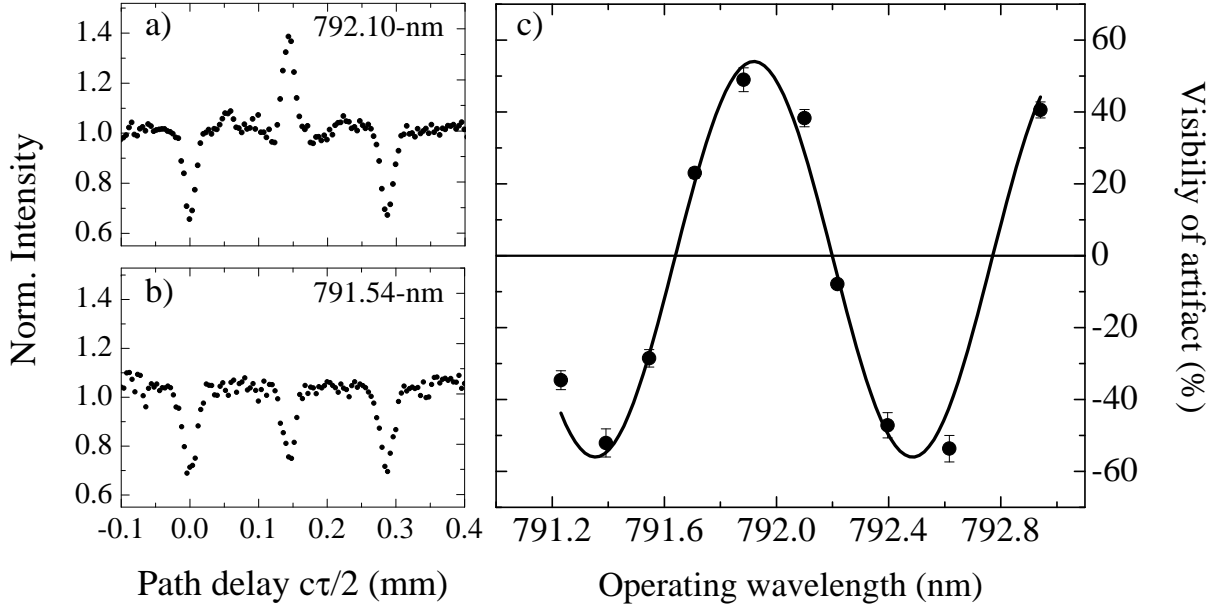


FIG. 4: Controlling the phase of the artifact. CPI interferograms of the sample taken at an operating wavelength of a) 792.10 nm and b) 791.54 nm clearly shows the dependence of the phase of the artifact interference on the operating wavelength. c) Visibility of the artifact versus operating wavelength. Positive (negative) visibility corresponds to constructive (destructive) interference. The measured period of oscillation of (1.13 ± 0.02) nm is in good agreement with the theoretical expectation.

lines, formed by the two doublets for varying path delay, cross at four distinct points. Two of these points occur at the same wavelength but at different path delays; they correspond to the dips in the CPI scans indicating real features of the sample. The other two crossing points occur at the same path delay but different wavelengths; these give rise to the artifacts.

As in Q-OCT, the interference giving rise to the artifacts can be constructive or destructive whereas for real features it is always destructive. If the interference is constructive, as in Fig. 2, the artifact is easy to identify. If instead it is destructive, artifacts can easily be confused with real features. In Q-OCT it was predicted that this could be adjusted by changing the sum-frequency of the entangled photon pair [4]. In practice, however, this is difficult as most UV narrow-band pump sources for SPDC are not tunable. CPI has the intrinsic advantage that the operating frequency is tunable by changing the relative delay between the chirped and anti-chirped pulses at the input beam splitter. In Figs. 4(a) and 4(b), we show two examples of CPI interferograms taken at different operating wavelengths 792.10 nm and 791.54 nm illustrating constructive and destructive interference in the artifact, respectively. The operating frequency is half the SFG frequency measured near zero delay. In these scans the path delay was not varied continuously but in discrete steps, accounting for fewer data points.

We employ the model transfer function for the coverslip, $H(\Omega) = r_1 + r_2 e^{i2k(\omega_0 + \Omega)d}$, where r_1 (r_2) is the reflection amplitude from the front (back) surface, $k(\omega)$ is the wavevector in the glass, and d is the thickness. Inserting this expression into Eq. (1), one finds that the

term describing the artifact is modulated by $\cos 2k(\omega_0)d$. If the operating frequency changes from ω_0 to $\omega_0 + \delta$, then $k(\omega_0 + \delta) \approx k(\omega_0) + \alpha\delta$ and the expected change in wavelength required to flip the sign of the artifact is $\Delta\lambda \approx \pi^2 c / (\omega_0^2 \alpha d)$.

Figure 4(c) shows the visibility of the artifact as a function of the operating wavelength. Visibility is defined as $(I_C - I_S)/I_S$, where I_C and I_S are the intensities at the centre of the dip and at the shoulder, respectively. A fit to this data yields a period of (1.13 ± 0.02) nm in good agreement with the theoretical prediction of 1.09 nm. Changing the operating wavelength in this straightforward way allows identification and removal of artifacts from axial scans.

There is a difference between Q-OCT and CPI. Even in the absence of dispersion, the resolution in Q-OCT is a factor of 2 better than in WLI [4] while, assuming Gaussian spectra, CPI has a factor of $\sqrt{2}$ better resolution than WLI. The difference originates from the effective bandwidths used in the comparison. Assuming a source of entangled photons with spectrum $S(\Omega)$ (the modulus squared of $\zeta(\Omega)$ in Eq. (5) in [4]), the effective bandwidths for HOM interference (see [4], Eq. (8)) and WLI (see [4], Eq. (4)) are the same because their spectra, $S(\Omega)$, are identical [15]. For chirped pulses with spectra $I(\Omega)$, the bandwidth for CPI is determined by $I(\Omega)I(-\Omega)$ (see Eq. (1)) while that for WLI is determined by $I(\Omega)$. For Gaussian spectra the effective bandwidth for CPI is $\sqrt{2}$ narrower than that for the WLI, accounting for the resolution advantage of Q-OCT.

Is this a fundamental feature of entanglement? Surprisingly no. The same difference in resolution could be achieved using purely classical correlations. In CPI, time-correlations, but not intensity correlations are created between anticorrelated frequencies. In the same setup, one replaces the chirped pulses with two CW lasers tuned to frequencies $\omega_0 + \Omega$ and $\omega_0 + \Omega'$. During the integration time of the detection the laser frequencies are swept in an anticorrelated way according to the distribution $P(\Omega, \Omega') = G(\Omega)\delta(\Omega + \Omega')$. In this case, the effective spectrum in Eq. (1) is $G(\Omega)$, while the WLI bandwidth is determined by the marginal $P(\Omega) = \int d\Omega' P(\Omega, \Omega') = G(\Omega)$. The effective bandwidths are identical in both cases and thus this classical scheme achieves the same factor of 2 higher resolution as Q-OCT. In practice, however, chirped pulses offer dramatically higher nonlinear conversion efficiency compared to CW lasers far outweighing this rather small difference.

CONCLUSION

We have shown that chirped-pulse interferometry accrues the benefits of quantum-OCT, but with a dramatic increase in signal, direct optical detection, and a straightforward means of identifying artifacts. We have experimentally demonstrated improved resolution in CPI over WLI with and without mismatched dispersion by up to a factor of 2.65. Increasing the bandwidth of the light source is required for the resolution in CPI-based OCT to compete with established techniques. Broadband (148nm) three-wave mixing of anticorrelated frequencies has been demonstrated in 1.5mm-thick nonlinear materials [16]. For safe *in vivo* imaging, the optical power can be attenuated before the sample without loss of signal visibility [11]. We have demonstrated SFG detection of reflected signals as low as 5mW [11]. Based on the results of [17], efficient SFG should be measureable with much lower reflected powers. Incorporating better nonlinear materials, such as PPKTP, and more sensitive detectors will further allow operation at lower power levels. CPI achieves the benefits of quantum interferometry at macroscopic power levels and represents a powerful new technique for optical imaging. More generally, we have clarified the role of entanglement versus correlation in

axial imaging.

Acknowledgements

We acknowledge financial support from NSERC and CFI. We thank G. Weihs and C. Couteau for the use of their spectrometer and technical assistance. We thank D. Biggerstaff, K. Bizheva, D. Strickland, and G. Weihs for valuable discussions. J.L. acknowledges financial support from the Bell Family Fund and R.K. acknowledges financial support from IQC and ORDCF.

* Electronic address: kresch@iqc.ca

- [1] J. G. Fujimoto, M. E. Brezinski, G. J. Tearney, S. A. Boppart, B. Bouma, M. R. Hee, J. F. Southern, and E. A. Swanson, "Optical biopsy and imaging using optical coherence tomography," *Nature Med.* **1**, 970-972 (1995).
- [2] A. F. Fercher, W. Drexler, C. K. Hitzenberger, and T. Lasser, "Optical coherence tomography - principles and applications," *Rep. Prog. Phys.* **66**, 239-303 (2003).
- [3] W. Drexler, "Ultrahigh-resolution optical coherence tomography," *J. Biomed. Opt.* **9**, 47-74 (2004).
- [4] A. F. Abouraddy, M. B. Nasr, B. E. A. Saleh, A. V. Sergienko, and M. C. Teich, "Quantum-optical coherence tomography with dispersion cancellation," *Phys. Rev. A* **65**, 053817 (2002).
- [5] M. B. Nasr, B. E. A. Saleh, A. V. Sergienko, and M. C. Teich, "Demonstration of Dispersion-Canceled Quantum-Optical Coherence Tomography," *Phys. Rev. Lett.* **91**, 083601 (2003).
- [6] C. K. Hong, Z. Y. Ou, and L. Mandel, "Measurement of subpicosecond time intervals between two photons by interference," *Phys. Rev. Lett.* **59**, 2044-2046 (1987).
- [7] A. M. Steinberg, P. G. Kwiat, and R. Y. Chiao, "Dispersion cancellation in a measurement of the single-photon propagation velocity in glass," *Phys. Rev. Lett.* **68**, 2421-2424 (1992).
- [8] B. I. Erkmen and J. H. Shapiro, "Phase-conjugate optical coherence tomography," *Phys. Rev. A* **74**, 041601 (2006).
- [9] K. Banaszek, A. S. Radunsky, and I. A. Walmsley, "Blind dispersion compensation for optical coherence tomography," *Opt. Commun.* **269**, 152-155 (2007).
- [10] K. J. Resch, P. Puvanathan, J. S. Lundeen, M. W. Mitchell, and K. Bizheva, "Classical dispersion-cancellation interferometry," *Opt. Express* **15**, 8797-8804 (2007).
- [11] R. Kaltenbaek, J. Lavoie, D. N. Biggerstaff, and K. J. Resch, "Quantum-inspired interferometry using chirped laser pulses," *Nat. Phys.* **4**, 864-868 (2008).
- [12] M. Pessot, P. Maine, and G. Mourou, "1000 times expansion/compression of optical pulses for chirped pulse amplification," *Opt. Commun.* **62**, 419-421 (1987).
- [13] J. Altepeter, E. Jeffreys, and P. Kwiat, "Phase-compensated ultra-bright source of entangled photons," *Opt. Express* **13**, 8951-8959 (2005).
- [14] Sellmeier coefficients, representative for Code 0211 microsheet glass, were provided by Corning Inc.
- [15] If the bandwidth in HOM interference is determined by a pair of Gaussian bandpass filters in front of the detectors, rather than by the source, then the HOM dip is narrower than the WLI by only a factor of $\sqrt{2}$.

- [16] S. Carrasco, M. B. Nasr, A. V. Sergienko, B. E. Saleh, M. C. Teich, J. P. Torres, and L. Torner, “Broadband light generation by noncollinear parametric downconversion” *Opt. Lett.* **31**, 253-255 (2006).
- [17] A. Pe’er, Y. Bromberg, B. Dayan, Y. Silberberg, and A. A. Friesem, “Broadband sum-frequency generation as an efficient two-photon detector for optical tomography” *Opt. Express* **15**, 8760-8769 (2007).